

Effects of Shielding Gas on the Mechanical and Microstructural Properties of 409L Ferritic Stainless Steels during Gas Metal Arc Welding

A. Fegghi¹, A. Emamikhah^{2,*}, Y. Bayat Asl²

¹Department of Materials Engineering, Najafabad Branch, Islamic Azad University, Isfahan, Iran.

²Department of Mechanical Engineering, Najafabad Branch, Islamic Azad University, Isfahan, Iran.

Received: 2 July 2017 - Accepted: 15 August 2017

Abstract

The present study investigates the effects of type of shielding gas on the weld microstructure and mechanical properties of 409L ferritic stainless steel. For this purpose, Ar, Ar +20% He, Ar + 12% CO₂, and Ar + 25% CO₂ were used as shielding gases in gas metal arc welding (GMAW) of stainless steel. To evaluate the welds, non-destructive inspections of the specimens were followed by mechanical (hardness and tensile) tests while microstructural examinations of both the heat affected zone (HAZ) and the fusion zone were performed. Moreover, the phases produced were observed and identified by analyzing the specimens using SEM and EDS techniques. Results showed that specimens welded with Ar + 25% CO₂ and Ar + 12% CO₂ have the highest strength and hardness values in the fusion zone due to the formation of martensite around the ferrite grains. However, the enhancements observed in the mechanical properties of specimens welded with Ar and Ar +20% He were attributed to the reduced ferrite grain size and martensite content.

Keyword: Ferritic Stainless Steels, Shielding Gas, Gas Metal Arc Welding, Microstructure, Mechanical Tests.

1. Introduction

The basic concept of GMAW (Gas Metal Arc Welding) was initially introduced in 1920s and the process has shown its advantages for welding a very wide range of materials with different thicknesses since the technique was first used in 1940s by aerospace companies for welding aluminum parts [1-2]. The process is well known among the welding fabricators across the globe for its advantages over the shielded metal arc welding (SMAW) [3]. For example, the electrode length in this technique does not face restrictions, thus allowing for longer welding lines to be welded in desired positions. Additionally, the higher welding speed in both automatic and semi-automatic modes and the higher deposition rate with deeper penetration and less operator skills have been referred to as additional advantages that enhance the applications of the GMAW process [4].

Although the basic principles of GMAW are already well established, research in the field still continues in an attempt to improve the process, and especially to gain control of the main process parameters for selecting the right ones that will lead to desired results. Shielding gas is one of the main GMAW parameters that play important roles in the welding process. Studies have shown the significant effects of shielding gas on protecting the molten metal, wire, and weld pool against atmospheric oxidation;

torch cooling; arc stabilization; uniform metal transfer; and enhanced quality, efficiency, and mechanical properties of the weld metal [5-6].

Many published studies have investigated the effects of different shielding gases, composition (gas blend), flow rate, geometry, and gas nozzle diameter on different weld materials [7-9]. Dreher et al. (2013) studied the shielding gas flow rate in the GMAW process to show that atmospheric contamination of the shielding gas was caused by turbulence due to the asymmetrical flow of shielding gas and torch design [10].

In view of the fact that penetration of oxygen and nitrogen weakens stainless steel subjected to GMAW, proper selection of the shielding gas is essential for achieving enhanced strength and corrosion resistance in the weld metal. The relationship between the type of shielding gas used and GMAW of stainless steel is rather complicated so that optimum results cannot be expected unless experiments are performed with different shielding gases to identify the right one(s) for each application. Argon (Ar), Helium (He), and CO₂ are commonly used for welding stainless steels of different compositions. Also, some studies have recommended the inclusion of a small quantity of oxygen in order to stabilize the arc and to prevent the weld pool from entering the carbon flow [11].

Ferritic stainless steels are alloys with the general composition formula of Fe-Cr-C that have adequate quantities of chromium in addition to other ferrite stabilizing elements such as aluminum, titanium, molybdenum, and niobium. The presence of ferrite stabilizing elements prevents the ferrite to transform

*Corresponding author

Email address: afshin.emamikhah@gmail.com

into austenite during heating; therefore, these types of steels are not heat-treatable. An important characteristic of these alloys is their good resistance against stress corrosion cracking (SCC), pitting corrosion, and grooving corrosion (especially in a chloride medium) [12-15]. Hence, ferritic stainless steels are useful for applications in which corrosion resistance is required or in working conditions that require enhanced mechanical properties such as toughness as well as ductility [16-18]. Regarding temperature limits, applications of ferritic stainless steel are limited to thermal operating conditions below 400 °C due to the formation of brittle phases. As regards metallurgical properties, the weld metal of these alloys is often ferritic although martensite may, in specific conditions, be present or carbides and nitrides might precipitate as well. The main concern in weldability of ferritic stainless steels is to ensure their toughness and ductility are preserved under the actual welding conditions.

AISI 409L (UNS 40900 or EN 1.4512) as one of the ferritic stainless steels with low chromium and carbon contents is reasonably resistant to both corrosion and oxidation. It is widely used in automotive exhaust systems, mufflers, and agricultural implements [19]. Hardening is drastically reduced due to heat treatment when the carbon content is low but that of titanium is high enough. Titanium not only helps the stabilization of steel during welding, but also prevents the formation of chromium carbide.

Most common welding methods can be used for welding 409L stainless steel. For example, Ahn et al (2012) employed friction stir welding (FSW) for welding 409L stainless steel using a silicon nitride tool. They demonstrated that the weld metal had the same mechanical properties as the base metal while no chromium carbide was observed in the weld metal after welding [20]. If the parameters involved are properly selected, GMAW will then be the right choice for welding 409L ferritic stainless steel.

In this experimental study, an in-depth investigation was carried out to determine the effects of type of shielding gas on the microstructure and mechanical properties of 409L ferritic stainless steel. In addition to mechanical tests, scanning electron microscopy (SEM) and energy dispersive spectrometry (EDS) were employed to investigate the formation of phases with the shielding gas as the variable while all other welding parameters were kept constants.

Mechanical and microstructural studies confirmed the important role of the shielding gas used during the GMAW of 409L ferritic stainless steel.

The gas blends used are in fact, currently being employed for manufacturing automotive exhaust pipes although the manufacturers do not have an accurately knowledge of the proportions of the gases in their blends. Capillary cracks along the body of the exhaust pipes thus manufactured have encouraged researchers to investigate and control the welding parameters involved.

2. Materials and Methods

Gas metal arc welding (GMAW) was performed on 409L ferritic stainless steel using different shielding gases. The chemical and mechanical properties of the 409L stainless steel used are presented in Tables 1 and 2, respectively. Experiments were iteratively performed on all the specimens in a closed welding workshop under identical environmental conditions and a constant temperature using a torch with a steady flow of the experimental gas blends operated in the automatic welding mode to determine the best gas blend for welding 409L ferritic stainless steel. Plates were precisely cut using a shearing machine 200×10×2.4 mm in dimensions according to ASME SECTION 9. The specimens were then cleaned and degreased before they were fitted within the fixture in a butt configuration. Given the fact that plates have a tendency to drift apart and that they may undergo distortion during the welding process, the initial and final points of the plates (i.e., the weld line) were firmly fixed using tack welds. This helped maintain the quality and the appearance of the welds practically intact throughout the welding process.

A common electrode (namely, ER-70S-6) with chemical properties identical to those of the base metal was used for welding the 409L plates (Table 3.). It has been shown that selecting electrodes with chemical properties similar to those of the base metal enhances the weld quality of stainless steels [21], apparently because this partly prevents the formation of phases other than the ferrite during the welding process while it also prevents vast variations in the toughness and ductility of the welded steel.

Table 1. Chemical composition of the 409L (wt. %) [14].

Fe	Cr	Si	C	S	P	Mn	Mo	V	Cu	Ni	W	Ti
Balance	11.50	0.60	0.01	0.01	0.01	0.30	0.03	0.16	0.05	0.06	0.03	0.16

Table 2. Mechanical properties of the 409L [14].

Tensile Strength (MPa)	Yield Strength (MPa)	Elongation (%)	Young Modulus (Gpa)	Poisson's Ratio
450	240	25	190-210	0.27-0.3

Table 3. Mechanical Properties and chemical composition (wt. %) of the ER-70S-6 [21].

Cr	Si	Mn	P	S	Tensile strength	Yield strength
0.06-0.15	0.8-1.15	1.4-1.85	<0.025	<0.025	500-640 N/m ²	420 N/m ²

Welding was accomplished automatically while such parameters as the velocity of the wire feeding rate, voltage, gas flow rate, and welding speed were varied in accordance with ASME SECTION 9 (Table 4.). The optimum welding parameters were thus selected as presented in Table 5. and the effects of shielding gases on 409 L plates were evaluated under constant welding conditions.

In this study, the effects of different gas proportions and blends were investigated on the weld life of exhaust pipes by changing the percent contents of the gases used in the blends. The optimum parameters were only determined after an adequately large number of experimental setups had been tested. The specimens manufactured under various test setups and with different gas blends were then visually inspected and compared with each other. Finally, the best ones were subjected to penetrant tests to ensure proper and accurate welding. Fig. 1. shows the specimens welded with Ar, Ar + 20% He, Ar + 12% CO₂ and Ar + 25% CO₂.

The specimens were subjected to mechanical and microstructural tests after the welding was over. Weld length, width, and height; HAZ (Heat Affected Zone) width; excess penetration; undercut; lack of fusion; reinforcement; spatter; lack of penetration; possible cracks; and appearance were visually evaluated in accordance with ASME

Standard. Standard liquid penetrant test was used to determine weld accuracy in all the specimens and unseen defects passing into the surface were identified.

Vickers micro-hardness test (HVS 1000) was performed using a 100-gr force at 10-s intervals on the weld metal, the base metal, and HAZ. Tensile tests were also performed on specimens 20×4×2.4cm in dimensions along the longitudinal and transverse directions in accordance with ASTM E8M under laboratory conditions (temperature: 21 °C; humidity: 33%) [22]. to verify the results of the tensile tests, two additional specimens were prepared for each weld setup (totally 16 specimens) performed under identical conditions.

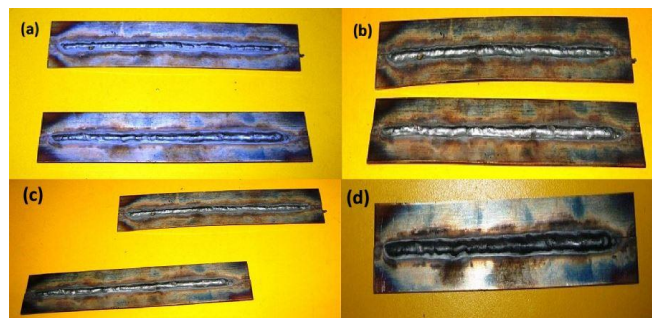
Optical microscopy (Olympus- CK 40M invert) was used with 200, 400, and 1000 magnifications to study the microstructure of the specimens as well as the changes that might have occurred in them due to welding. Different solutions were used in the etching process to bring about changes in the chemical composition of the weld metal that would make it different from the base metal. For this purpose, an initial solution was used for etching the weld metal, but a solution of equal amounts of HCL, HNO₃, and ascetic acid were used for etching the base metal. Finally, the welding area was analyzed using SEM (LEO- 435 VP) and EDS to identify the phases produced.

Table 4. Selecting parameters for GMAW of 409L according to ASME SECTION 9.

Shielding gas	Plate thickness (mm)	Amperage (A)	Voltage (V)	Wire feeding rate (cm/min)	Gas flow rate (lit/min)
Ar	1-1.5	50-120	16-19	250-550	10-14
Ar + He	1-1.5	40-145	16-18	300-475	10-15
Ar + CO ₂	1-1.5	130-140	15-21	90-440	10-17

Table 5. Extracted parameters for GMAW of 409L.

Shielding gas	Gas flow rate (lit/min)	Voltage (V)	Wire feeding rate (cm/min)	Plate thickness	Welding mode
Ar	12	16	375	2.4	Automatic
Ar + 20% He	12	16	375	2.4	Automatic
Ar + 12% CO ₂	12	16	375	2.4	Automatic
Ar + 25% CO ₂	12	16	375	2.4	Automatic

**Fig. 1. Specimens welded with (a) Ar, (b) Ar + 20% He, (c) Ar + 12% CO₂, and (d) Ar + 25% CO₂.**

3. Results and Discussion

Non-destructive examinations (i.e., visual and liquid penetrant tests) of the specimens yielded expected results, confirming the quality of all the welds in terms of appearance and possible defects (Table 6.). The results obtained from micro-hardness tests are presented in Fig. 2. Clearly, HAZ hardness decreased in all the specimens as compared with the base metal. The hardness of the weld metal, however, exhibited a great increase in all the specimens. The hardness observed in the weld metal was the highest with 290 HVS when Ar + 25% CO₂ shielding gas was used. This was followed by Ar + 15% CO₂ (278 HVS), Ar + 20% He, and Ar in a descending order.

Tables 7 and 8. gives the result of transverse and longitudinal tensile test, respectively. Clearly, the specimens welded with Ar + 25% CO₂ shielding gas yielded the highest tensile strength under the longitudinal tensile test; in the transverse tensile test, however, all the specimens fractured from their HAZ zones while approximately the same results were obtained for both ultimate tensile strength and yield strength.

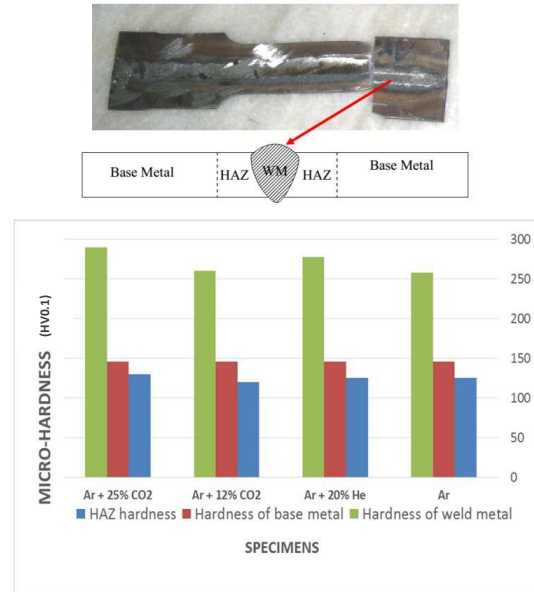


Fig. 2. Maximum hardness of the specimens.

Table 6. Results of visual test.

Shielding gas	Weld height (mm)	Weld width (mm)	HAZ width (mm)	Visual defects	Appearance	Image of defects
Ar	5	6.5	5	Low porosity and spatter	Without defect	-
Ar + 20% He	4	7	6	Low porosity and spatter	Low weld reinforcement	
Ar + 12% CO ₂	2	10	9	High width of weld, low height of weld, and high penetration	Low weld reinforcement	
Ar + 25% CO ₂	3	9	8	High spark and spatter	High spatter	

Table 7. Results of transverse tensile test.

Shielding gas	Tensile Strength (Mpa)	Yield Strength (Mpa)	Location of fracture
Ar	475	342	HAZ
Ar + 20% He	469	341	HAZ
Ar + 12% CO ₂	464	340	HAZ
Ar + 25% CO ₂	481	345	HAZ

Table 8. Results of longitudinal tensile test.

Shielding gas	Ultimate Tensile Strength (Mpa)	Yield Strength (Mpa)	Location of fracture
Ar	528	395	Weld metal
Ar + 20% He	548	408	Weld metal
Ar + 12% CO ₂	493	385	Weld metal
Ar + 25% CO ₂	581	438	Weld metal

Fig. 3. depicts the relationship between the type of shielding gas and the width of the HAZ area. Obviously, HAZ width increased as a result of adding CO₂ to Ar. The highest HAZ width was obtained for specimens welded with Ar + He gas. The increased HAZ width as a result of adding the mixed gas (He or CO₂) is due to the rise in arc energy [23-25].

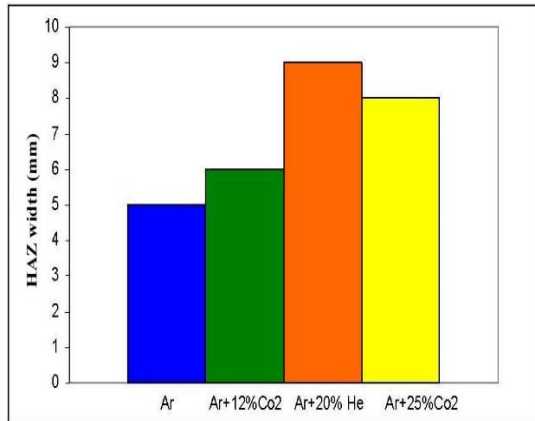


Fig. 3. Ratio of shielding gas to HAZ width.

Generally, the energy of ionization potential and the enthalpy of arc column increased by adding CO₂ or He to Ar, which resulted in enhanced arc energy and, thereby, in increased HAZ width. These parameters also increased weld penetration [4, 26]. Fig. 4. shows the effect of shielding gas on height/width ratio of weld reinforcement. Here again, the height/width ratio increased due to the increased energy of the arc column when CO₂ and He were added to Ar.

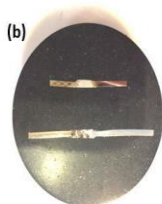
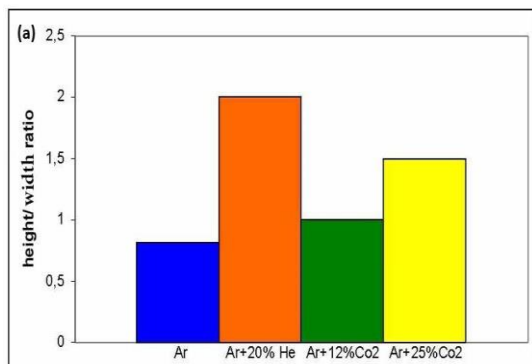


Fig. 4. (a) Effect of shielding gas on height/width ratio of the weld reinforcement, (b) cross section sample of Ar + 20% He.

Our investigations show that low chromium ferritic stainless steels (10.5 ~ 12.5% Cr) are used in such applications as automotive exhaust system due to its corrosion resistance properties compared to those of carbon steels. The thermal limit of ferritic stainless steel is below 400 °C because of its ability to form brittle phases. From a metallurgical point of view, the weld metal in these alloys is often ferritic. However, under special conditions, martensite may also be present in addition to carbides and nitrides. The main advantage of ferritic stainless steels is their capability to preserve toughness and adequate ductility under as-welded conditions.

It is necessary to determine which of the base metals of ferritic stainless steels, such as 405 or 409, lacks in martensite. The presence or absence of martensite can be judged by K-factors greater than 13.5 [27]. Based on Equation 1, the base metal lacks martensite and the steel is completely ferritic, as also evidenced by microscopic examinations.

$$\text{K-factor} = \text{Cr} + 6\text{Si} + 8\text{Ti} + 21\text{Al} - 40(\text{C} + \text{N}) - 2\text{Mn} - 4\text{Ni} = 13.8 \quad (1)$$

Fig. 5. shows the microstructure of the completely ferritic 409L used in this study.

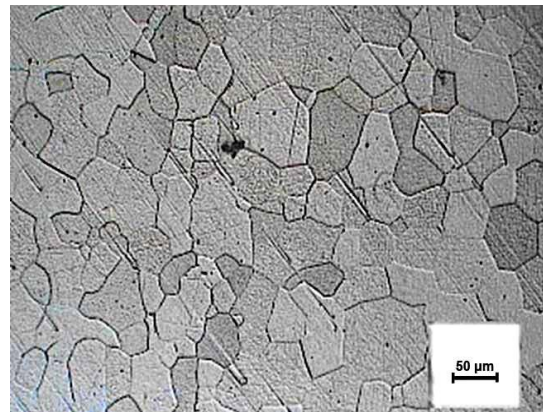
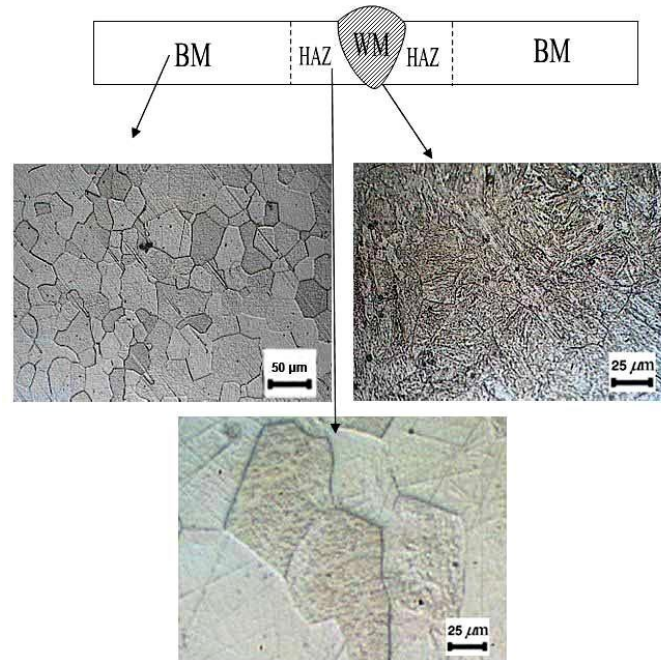


Fig. 5. Microstructure of 409L stainless steel employed.

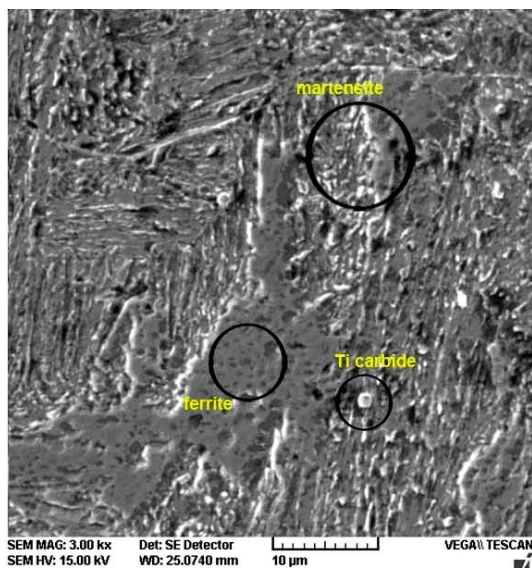
Microstructural investigations were conducted using optical microscopy (OM) to determine the hardness and strength of the welded specimens. Table 9. indicates the microstructure of weld metals of all specimens. Fig. 6. shows the microstructure of the specimen welded with Ar + 25%CO₂ shielding gas. Based on the analysis, the heat affected zone (HAZ) in all the specimens grew with increasing ferritic grain size and, as expected, no phase alternations were observed. Based on the hardness results obtained and according to the Hall-Petch theory, the increase in ferrite grain size must be one reason for the observed decrease in hardness. Moreover, no M₂₃C₆ or M₂₃(C, N)₆ carbides precipitated in the microstructure of HAZ, perhaps due to the low chromium content and the presence of titanium which reacted with carbon and nitrogen.

Table 9. The microstructure of weld metals.

Shielding gas	Ar	Ar + 20% He	Ar + 12% CO ₂	Ar + 25% CO ₂
Microstructure of weld metal	Acicular and fine ferrite grains	fine ferrite grains	Acicular ferrite along with fine and low martensite	Acicular ferrite with more martensite

**Fig. 6. Microstructure of specimens welded with Ar + 25%CO₂ shielding gas.**

In spite of the favorable conditions observed in the HAZ area, variations were noticed in the weld metal, especially in specimens welded with Ar + 25%CO₂ and Ar + 12%CO₂. SEM analysis revealed that the microstructure of the specimens welded with Ar + 12%CO₂ were acicular and contained fine martensite (Fig. 7.).

**Fig. 7. SEM analysis of specimens welded with Ar + 12%CO₂.**

However, the microstructure of the specimen welded with Ar + 25%CO₂ was similar to that of the one welded with Ar + 12%CO₂, but only with a higher martensite content. Thus, the enhanced CO₂ to Ar ratio increased the likelihood of martensite formation and, consequently, enhanced the specimen's hardness and strength.

In fact, the presence of alloying elements in steel drastically increases the size of the austenite zone and affects the microstructure of ferritic stainless steels regardless of whether the alloying elements are added to or already exist as impurities in the steel. The presence of carbon due to the diffusion of Ar + 25%CO₂ shielding gas, therefore, helps the extent of the austenite zone to increase during welding at high temperatures with the consequent martensite formation during cooling to room temperature.

Studies have shown that martensite can leave both negative and positive effects on the mechanical properties of ferritic stainless steels. Regarding the carbon content and percent volume of the already existing martensite, the martensite phase formed in ferritic stainless steels is generally low in carbon and its hardness is below 30 HRC [28]. At temperatures at which austenite is stable, the martensite phase separates from the ferrite due to the greater diffusion of carbon into the austenite. Thus, it will be possible to raise martensite hardness

to 50 HRC by fast cooling of the weld to room temperature. However, the martensite phase formed in the steel does not reach these hardness values due to the short diffusion time.

Studies show that the martensite-ferrite boundary is susceptible to stress corrosion cracking (SCC) [29]. Therefore, ferritic stainless steels with martensite due to welding must be heat treated to temperatures between 760 to 815°C in order for them to reach optimum formability and corrosion properties [30]. This operation transmutes the martensite into ferrite and sphere carbides. This finding is further confirmed by the absence of CO₂ in Ar and Ar + 20%He shielding gases and the trivial amounts of martensite in the microstructure thus obtained. Hence, the increasing strength and hardness of the specimens welded through the use of shielding gases without CO₂ must be related to the enhanced cooling time, the reduced ferritic grain size, and the acicular structures formed (Fig. 8.). However, the presence of even low values of carbon in the electrode increases the likelihood of martensite formation in the weld metal.

It should be noted that researchers have shown that reduced chromium content in ferritic stainless steels deteriorates their corrosion resistance [11, 28]. This is because chromium rapidly penetrates into the ferrite at temperatures in the range of 700-925 °C to contribute to the precipitation of chromium carbide, which leads to reducing chromium amounts at grain boundaries and, thereby, to intergranular corrosion. EDS results indicate that the specimens face a drastic decrease in chromium content upon welding and this assumes a rising trend with increasing CO₂ content (Fig. 9.). Based on the EDS diagrams, the presence of titanium carbide becomes visible in the structure when CO₂ is added to Ar. Some studies have indicated that chromium carbide may also be present; the verification of this claim, however, requires TEM analysis for accurate observation and recognition.

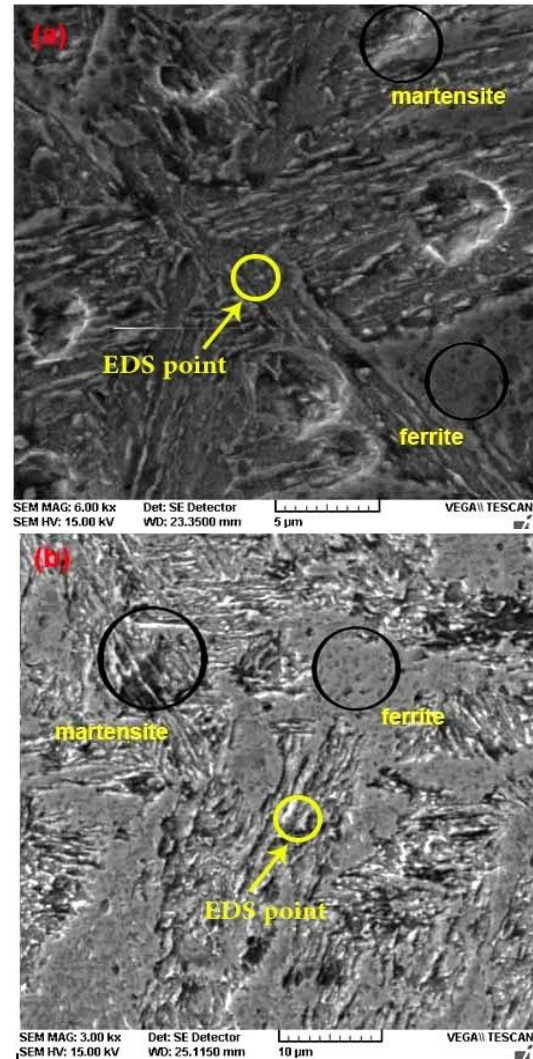


Fig. 8. SEM analysis of specimens welded with (a) Ar, and (b) Ar +20%He.

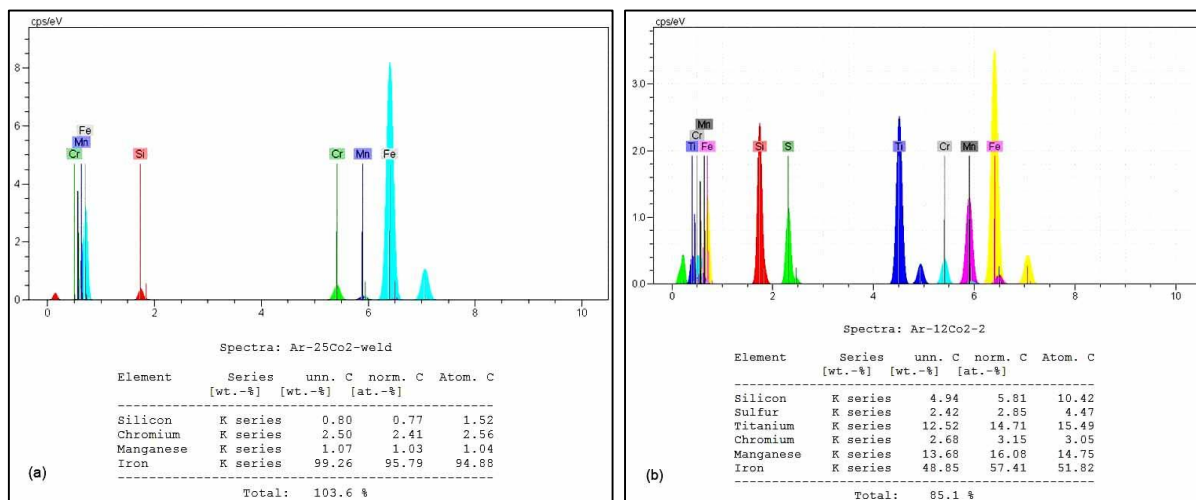


Fig. 9. EDS analysis of specimens welded with (a) Ar + 25%CO₂, and (b) Ar + 12%CO₂.

The intergranular corrosion mechanism is based on the precipitation of chromium carbide and the reduction of chromium in the adjacent grains [31] since corrosion is enhanced as a result of reduced chromium content.

4. Conclusions

Different shielding gases were used in welding ferritic stainless steel specimens and pot-tests were performed to determine the effects of the different shielding gases on the mechanical and microstructural properties of 409L ferritic stainless steels. Results indicate that high quality welds may be obtained by precisely controlling the carbon content in the base metal, the electrode, and the shielding gas. Moreover, desirable mechanical and microstructural properties are obtained if proper amounts of CO₂ are added to Ar in each case. The following conclusions may be drawn from the results obtained:

1. Specimens welded with Ar + 25% CO₂ and Ar + 12% CO₂ exhibited higher values of Vickers micro-hardness in the fusion zone than the base metal due to the formation of a martensite phase. Moreover, increasing the CO₂/Ar ratio was found to increase the martensite formed. The martensite content was lower in specimens welded with Ar +12% CO₂.
2. The enhanced strength and hardness observed in the specimens welded with Ar and Ar + 20%He without CO₂ could be attributed to the longer cooling time and to the formation of acicular ferrite grains accompanying the decreasing ferrite grain size.
3. Ferrite grain size increased in the HAZ area and all the specimens, consequently, recorded lower hardness values in this zone as compared to the base metal.
4. The results obtained from EDS analysis indicate that the specimens faced chromium depletion upon welding; the depletion increased with increasing CO₂ content.
5. Adding CO₂ or He to Ar was found to increase weld penetration and height/width ratio due to the increased energy of the arc column.

References

- [1] T. Varga, T. Konkoly and H. Straube: Investigation on microstructure, toughness, and defect tolerance of gas metal arc weld metal, IIW. Doc., X-1205-90, (1990).
- [2] P. Kah, R. Suoranta and J. Martikainen. Int. J. Adv. Manuf. Technol., 67(2013), 655.
- [3] B. Mvola, P. Kah, J. Martikainen, and R. Suoranta, J. Eng. Manu. Part B., 229(2015), 1694.
- [4] ASM handbook. Welding, brazing, and soldering, ASM, Cleveland, (1993).
- [5] S.W. Campbell, F.H. Ley, A.M. Galloway and N. McPherson, J. Eng. Manu. Part B., 229(2015), 122.
- [6] C. Kim, J. Eng. Manu. Part B., 229(2015), 1557.
- [7] S. Mukhopadhyay, T. K. Pal, Int. J. Adv. Manuf. Technol., 29(2005), 262.
- [8] V. V. Vaidya, Weld. J., 81(2002), 43.
- [9] S. Lathabai, R. D. Stout, Weld. J., 64(1985), 303.
- [10] M. Dreher, S. Fussel, S. Rose, M. Habler, M. Hertel and M. Schnick, Int. J. Adv. Manuf. Technol. 57(2013), 391.
- [11] R. C. Cochrane, P. R. Kirkwood, In Proc of the Int Conf on Trends in Steel and Consumables for Welding, the Welding Institute, London, (1978), 103.
- [12] L. Pires, L. Quintino and R. M. Miranda, Mater. Des., 28(2007), 1623.
- [13] C. J. Niekerk, M. Toit and M. W. Erwee, Welding in the World, 56(2012), 54.
- [14] AWS Welding handbook. Stainless steels. (1997), 4.
- [15] Y. Uematsu, N. Hiramatsu and M. Oku, US5462611 A 1995. International Patent Application No. US/08356, 248.
- [16] V. Kuzucu, M. Aksoy, M. H. Korkut and M.M.Yildirim, Mater. Sci. Eng. A, 230(1997), 75.
- [17] R. T. J. Hodges, j. Corros. Sci. Eng., 27(1971), 119.
- [18] H. K. D. H. Behadeshia. Mater. Sci. Forum., 539-543(2007), 6.
- [19] A. Miyazaki, M. Gunzi and K. Yoshioka, Kawasaki. Steel. Tech. Rep., 15(1994), 21.
- [20] B. W. Ahn, D. H. Choi, D. J. Kim, S.B. Jung, Mater. Sci. Eng. A, 532(2012), 476.
- [21] D. A. Brandt, J. C. Warner: Metallurgy Fundamentals, 5th Edition, Goodheart-Willcox Publisher, (2009).
- [22] Standard test Method for Tension Testing of Metallic Materials (1998) ASTM E 8M Annual Book of ASTM Standards, Part 8; ASTM.
- [23] F. Mohammadi, F. Eliyan and A. Alfantazi, Corros. Sci., 63(2012), 323.
- [24] H. Y. Liou, R. L. Hsieh and W. T. Tsai, Corros. Sci., 44(2002), 2841.
- [25] S. Kumar, A. S. Shahi, Mater. Des., 32(2011), 3617.
- [26] Z. H. Rao, S. M. Liao and H. L. Tsai, J. Appl. Phys., 107(2010), 044902.
- [27] J. C. Lippold, D. J. Kotecki: Welding metallurgy and weldability of stainless steels. Wiley publications, (2005).
- [28] A. K. Lakshminarayanan, V. Balasubramanian, Mater. Des., 31(2010), 4592.
- [29] C. L. Briant, S. K. Banerji, Int. Mater. Rev., 23(1978) 164.
- [30] A. J. Sedriks: Corrosion of stainless steels. Wiley Publications, (1996).
- [31] J. K. Kim, Y. H. Kim, S. H. Uhm, J. S. Lee, and K. Y. Kim, Corros. Sci., 51(2009), 2716.